Supplementary Materials

Molecular imaging of deoxycytidine kinase activity using deoxycytidine-enhanced CEST MRI

Zheng Han[1], Yuguo Li[1,2], Jia Zhang[1], Jing Liu[1,3], Chuheng Chen[4], Peter C. van Zijl[1,2], and Guanshu Liu[1,2,] *

[1]: Department of Radiology, Johns Hopkins University, Baltimore, MD, USA

[2]: F.M. Kirby Research Center for Functional Brain Imaging, Kennedy Krieger Institute, Baltimore, MD, USA

[3:] Radiology College, Guizhou Medical University, Guiyang, Guizhou P.R., China

[4]: Department of Biomedical Engineering, Johns Hopkins University, Baltimore, MD, USA

*To whom correspondence should be addressed: Dr. Guanshu Liu (guanshu@mri.jhu.edu)

Running title: CEST MRI of DCK enzyme activity

S1. In vitro characterization of the CEST MRI properties of dCTP

As shown in Fig S1, we characterized the pH and B1 dependence of the CEST signal of dCTP. While the CEST signals are stronger at low pH values, e.g. MTR_{asym}= 11.7±0.04% at pH 6.0 (for 5 mM dCTP in PBS solution, 37 ºC, B_1= 3.6μT), the CEST signals in the neutral pH range are still high enough, e.g. MTR_{asym}= 8.86±0.14% at pH 7.4, allowing the CEST MRI detection of intracellularly accumulated dC/dCTP. Yet, the accurate quantification of dC that distributes in the extracellular space is challenging as the extracellular pH in the tumor is acidic. Fortunately, such a technical challenge can be overcome by observing the CEST signal at an extended time window (e.g. > 30 min in our study) when dC is cleared from the tumor body sufficiently.

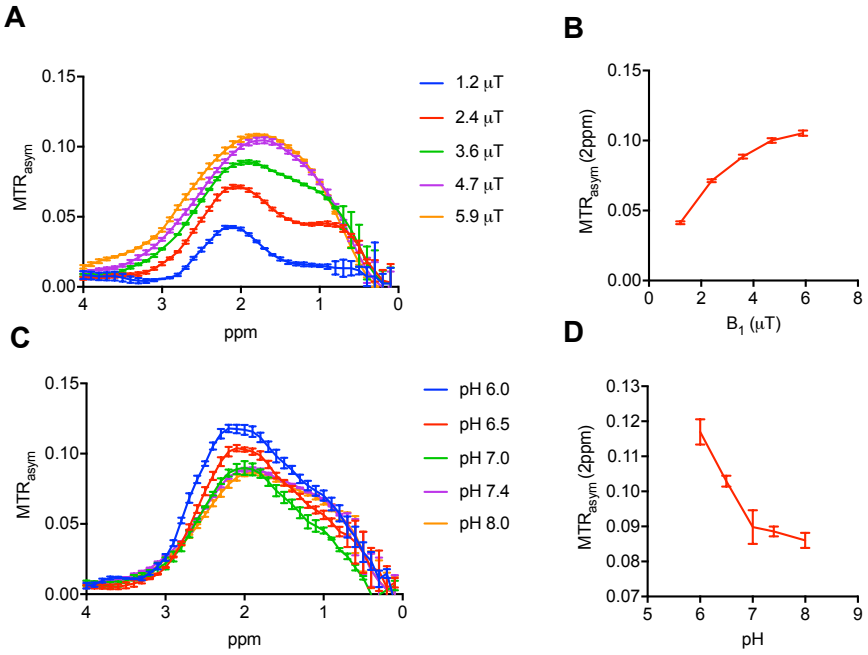

Figure S1. B_1 and pH dependence of the CEST MRI signal of dCTP. (A). MTR_{asym} of dCTP for B_1-values of 1., 2.4, 3.6, 4.7 and 5.9 μT at pH=7.4 (n=3). (B) B_1 dependence of MTR_{asym} of dCTP at pH=7.4 at 2 ppm (n=3). (C) MTR_{asym} of dCTP at pH 6.0, 6.5, 7.0, 7.4 and 8.0 using B_1

=3.6 μT (n=3). (D)**.** pH dependence of MTR_{asym} at 2 ppm using B_1 =3.6 μT (n=3). All data are presented as mean±SEM of 3 independent measurements (n=3).

Then we measured the CEST signal of dCTP solutions of 0.01 to 5 mM to determine the possible detection limit at pH 7.4 and 37°C at our acquisition condistions. The result is shown in Fig S2.

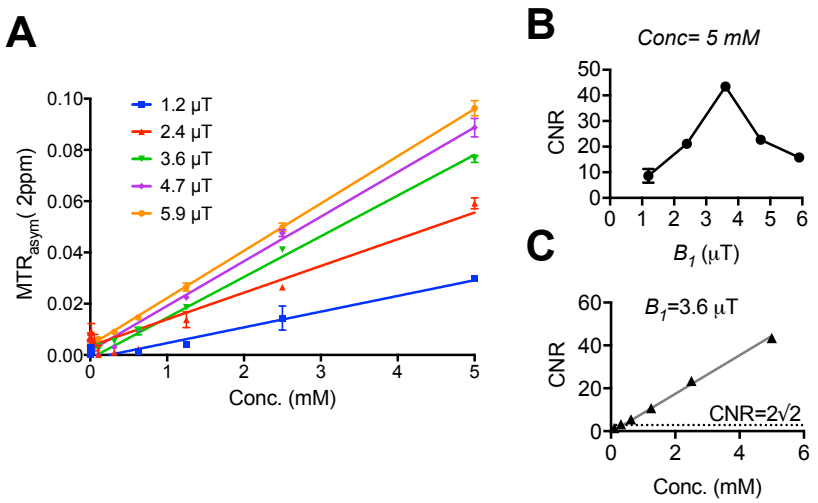

Figure S2. CEST MRI detectability of dCTP in solution. (A) MTR_{asym} values and their linear regression as a function of dCTP concentration (3.3 μM to 5 mM) at B_1=1.2, 2.4, 3.6, 4.7 and 5.9 μT (n=3). **(B)** B_1 dependence of CNR of 5 mM dCTP solution. CNR is defined by (MTR_{asym} (2 ppm, dCTP)- MTR_{asym} (2 ppm, PBS)) /noise, where noise is standard deviation of MTR_{asym} (2 ppm, PBS) at the corresponding B_1. **(C)** CNR at different concentration of dCTP at B_1= 3.6 μT. The CEST MRI detectability is defined as the minimal concentration of dCTP to obtain CNR $>2\sqrt{2}$ (1). Our result showed that the CEST MRI detectability of dCTP was 378 μM.

S2. NMR measurement of dC/ dCTP in L1210-WT cells

To quantify dC/dCTP concentration in the cells, we performed high resolution NMR on cell extracts of 1.5×10^6 L1210-WT cells with or without the incubation of 5 mM dC (24h). in brief, after washing with PBS twice, 1×10^7 cells were pelleted and used for preparing cell extracts using the methanol–chloroform–water extraction method (2, 3). Cell extracts were then diluted to 400 μL in D_2O with 5 mM DSS (4,4-dimethyl-4-silapentane-1-sulfonic acid) was used as an internal standard. NMR spectra were acquired using a Bruker 750 MHz, AVANCE III spectrometer (Bruker) equipped with a double-resonance 5 mm Inverse broadband (BBI) probe at 300 K, using the zgpr pulse sequence (single 90° pulse experiment with water suppression), with 128 transients collected into 65,536 (64 K) data points over a spectral width of 9765.625 Hz (13 ppm), acquisition time of 8.0 s, and relaxation delay of 6.5 s. Spectra were processed using Topsin 3.0 (Bruker) with an exponential line broadening of 20 Hz prior to Fourier transformation and automatic phase and baseline correction. DSS (4,4-dimethyl-4-silapentane-1-sulfonic acid, 5 mM, Sigma-Aldrich), which has a peak at 0.00 ppm, was used as a concentration and chemical shift reference.

The measured NMR spectra are shown Fig S3. To determine the concentration of dC/dCTP, we used the peak area at ~7.85 ppm, one of the dC/dCTP characteristic peaks according to previous reports. Calculation of dC/dCTP concentration was conducted by the ratio of the peak area between 7.8- 7.9 with respect to that of DSS (5 mM) at 0 ppm. The concentration of dC/dCTP of L1210-WT cells without (blue line) and with dC incubation (red line) was 0.208 and 1.361 nmol/10^6 cells, respectively. The corresponding intracellular concentrations are 0.39 and 2.6 mM, respectively, as calculated by assuming the average tumor cell has a diameter of 10 μm (Fig.S3A). In contrast, the concentration of dC/dCTP of L1210-10K cells without (blue line) and with dC incubation (red line) was 0.161 and 0.388 nmol/10^6 cells,

respectively. The corresponding intracellular concentration are 0.308 and 0.742 mM, respectively (Fig.S3B).

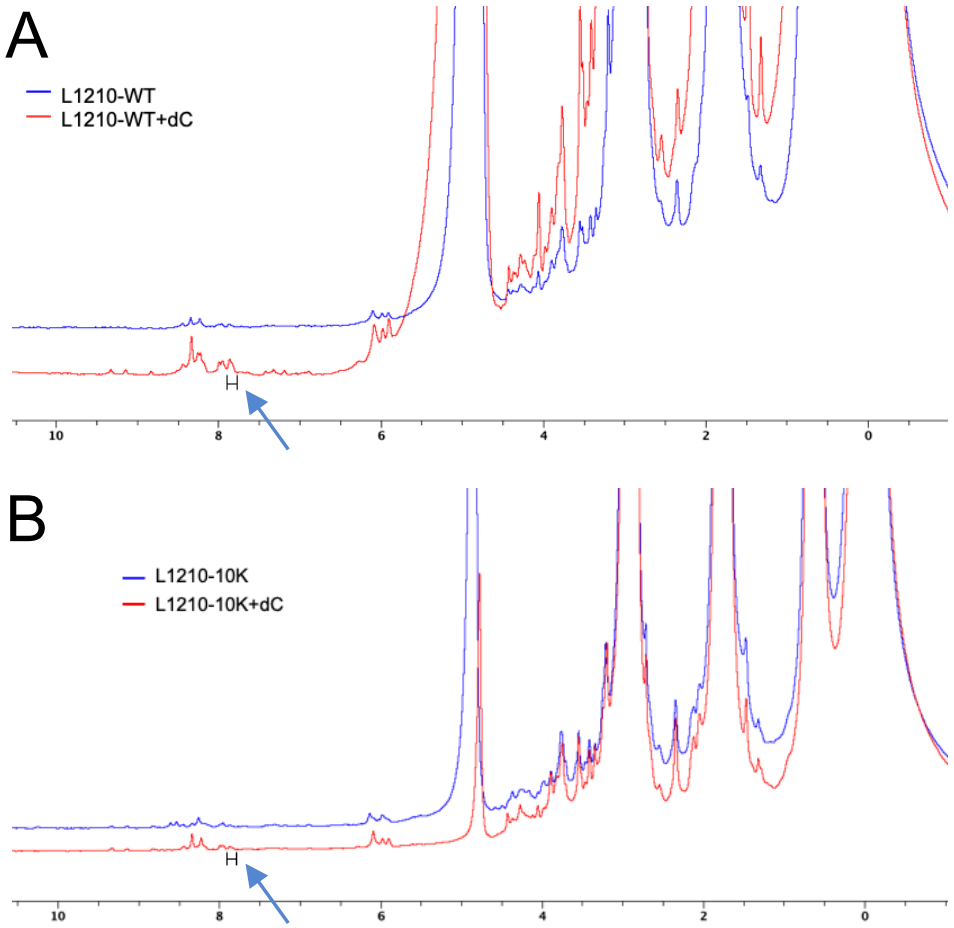

Figure S3. High-resolution NMR (750 MHz) of cell extracts of (A) L1210-WT and (B) L1210-10K with or without incubation with 5 mM dC for 24h. Note that the intensity of the two NMR spectra were adjusted by the peak height of DSS.

S3. The dynamic dC-enhanced CEST MRI maps

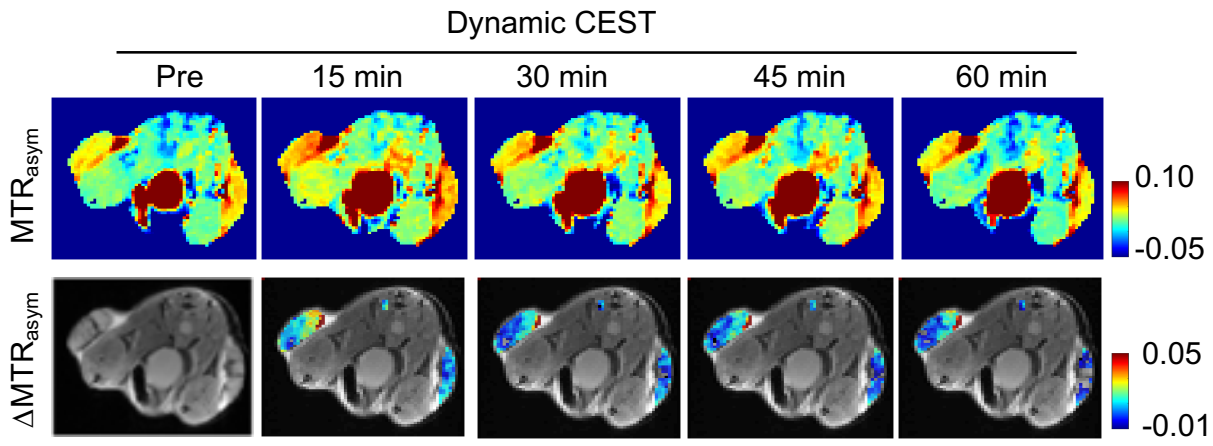

Figure S4. Representative dynamic CEST images. Representative MTRasym maps at 2.0 ppm at different time points pre and post treatment (top) and ΔMTRasym difference maps calculated from MTRasym(t)-MTRasym(pre). The ΔMTRasym maps were overlaid on the T_2w image and only intensities in the two tumors and muscle ROI are shown.

S4. Quantification of the tumor uptake of dC using T1-corrected CEST metric AREX.

To eliminate the potential influence by T_1 change after injection, we also calculated the AREX values in both tumors. As shown in Fig. S5, the mean AREX of L1210-WT tumor increased from 0.148 to 0.191, with a significant net increase of 0.044 or 29.6% relative signal change (p=0.0140), whereas that of L1210-10K tumor changed from 0.297 to 0.309, corresponding to a net increase of 0.012 or 4% relative signal change (p=0.6023).

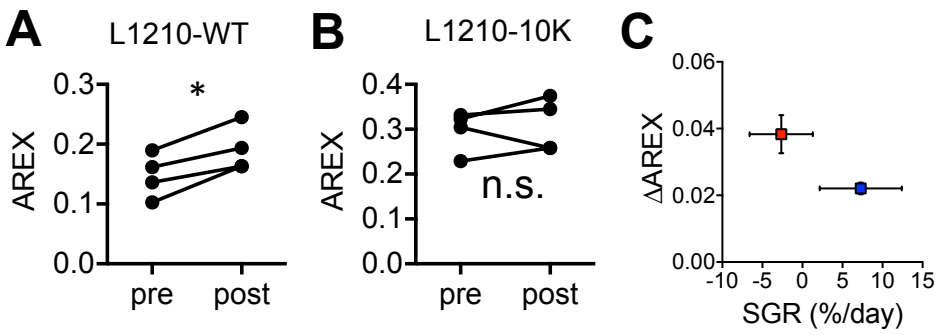

Figure S5. CEST MRI assessment of tumor uptake of dC using T_1-corrected CEST metric AREX. (A) and **(B)** Scatter plots of the pre- and post-injection AREX values of four L1210-WT and four L1210-10K tumors, respectively. *: $p<0.05$. n.s.: not significant (two-tailed paired Student's t-test, n=4). **(C)** Correlation between the mean CEST (ΔAREX) and specific growth rate for L1210-WT and L1210-10K tumors respectively. Errors are the standard deviations of the measured ΔAREX (n=4) and specific growth rate (n=5). Red box: L1210-WT; blue box: L1210-10K.

S5. CD31 Stains

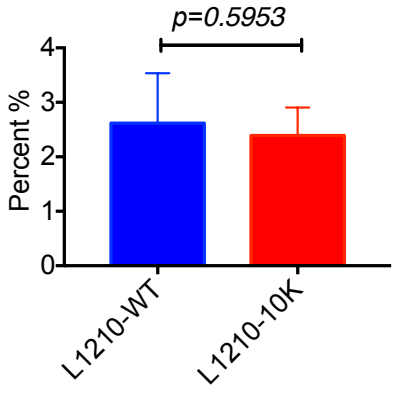

Figure S6. Comparison of the relative fluorescence intensities of CD31 staining of L1210-WT and 10K tumors (two-tailed paired Student's, n=3).

Reference

1. Brown RW, Haacke EM, Cheng Y-CN, Thompson MR, Venkatesan R. Magnetic resonance imaging: Physical principles and sequence design: John Wiley & Sons; 2014.
2. Le Belle JE, Harris NG, Williams SR, Bhakoo KK. A comparison of cell and tissue extraction techniques using high-resolution 1H-NMR spectroscopy. NMR Biomed. 2002;15:37-44.
3. Beckonert O, Keun HC, Ebbels TM, Bundy J, Holmes E, Lindon JC, et al. Metabolic profiling, metabolomic and metabonomic procedures for NMR spectroscopy of urine, plasma, serum and tissue extracts. Nat Protoc. 2007;2:2692-703.
4. Li Y, Qiao Y, Chen H, Bai R, Staedtke V, Han Z, et al. Characterization of tumor vascular permeability using natural dextrans and CEST MRI. Magn Reson Med. 2018;79:1001-9.
5. Cardenas-Rodriguez J, Howison CM, Pagel MD. A linear algorithm of the reference region model for DCE-MRI is robust and relaxes requirements for temporal resolution. Magn Reson Imaging. 2013;31:497-507.